23rd ABCM International Congress of Mechanical Engineering
December 6-11, 2015, Rio de Janeiro, RJ, Brazil

ELUCIDATING THE EFFECT OF CONTACT STRESSES IN DISSIMILAR ALUMINUM-TO-ALUMINUM JOINING VIA SELF-PIERCE RIVETING

J.F.C. Moraes
Department of Mechanical Engineering, The University of Alabama, Box 270276, Tuscaloosa AL 35487-0276
jfmoraes@crimson.ua.edu
H.M. Rao
Department of Mechanical Engineering, The University of Alabama, Box 270276, Tuscaloosa AL 35487-0276
hmrao@crimson.ua.edu
J.B. Jordon
Department of Mechanical Engineering, The University of Alabama, Box 270276, Tuscaloosa AL 35487-0276
bjordon@eng.ua.edu

Abstract. *In the present work, the relationship between residual stresses, contact forces and fatigue damage was studied for joining sheets of aluminum alloy 6111 to 5754 series by self-pierce riveting (SPR). To achieve this, an isotropic material hardening model with Johnson-Cook criterion was applied to simulate the SPR process via finite element analysis (FEA). Results from FEA indicated a strong relationship between the contact forces as a result of the SPR process and the fatigue crack initiation sites observed in the fatigue experiments. In fact, under high cycle fatigue, results indicate that fatigue cracks typically originated at areas of high contact forces, such that final rupture of the joint occurred away from the rivet.*

Keywords: *self-pierce riveting, FEA, fatigue*

1. INTRODUCTION

There is increased demand by both the governments and consumers around the globe for automobiles with improved fuel economy and safety (Miller et al. 2000). The use of lightweight aluminum alloys by replacing traditional heavy steel based alloys has been an ongoing challenge for the auto industry. The use of aluminum becomes particularly challenging when it comes to joining methods, as the traditional resistant spot welding (RSW) is not very feasible for use in automobile manufacturing. The alternative joining technique that has emerged to RSW is the self-piercing riveted (SPR) joining technique. SPR, a high speed mechanical fastening technique has been increasingly used to join aluminum and hard to weld materials (Cai et al. 2005; Litherland 1998). In this joining technique, a tubular rivet is pierced completely through the top sheet, generally called as pierced sheet and partially through the bottom overlapping sheet (locked sheet), which are held against a circular die of asymmetrical cavity. SPR has been studied widely and implemented by several auto manufacturers as one of the economical techniques to join aluminum extensive vehicle bodies (Mortimer 2001; Huang, J. Lasecki, et al. 2014; Barnes & Pashby 2000a; Barnes & Pashby 2000b; Cai et al. 2005).

Several studies have been conducted on fatigue behavior and fracture mechanisms of SPR joints of similar aluminum-to-aluminum (Chen et al. 2003; Fu & Mallick 2003; Han, Chrysanthou & O'Sullivan 2006; Iyer et al. 2005; Pickin et al. 2007) and aluminum-to-steel alloys (Abe et al. 2009; Han & Chrysanthou 2008; Han et al. 2007; Sun et al. 2007; Huang, J. Lasecki, et al. 2014). It is well documented that a relative motion between two surfaces which are clamped or held closely, results in fretting wear (Waterhouse 1984; Hurricks 1970). Similarly, in SPR joints, fretting can substantially decrease the fatigue life of the riveted joints. In aluminum alloy 5754 sheets joined by SPR, multiple fretting wear occurred between the faying surfaces of the sheets and between the rivet and the bottom sheet. Fretting debris consisting of fine oxide particles where observed at fretting area. In all the instances, fretting wear initiated micro-cracks, which eventually grew into dominant long cracks resulting in failure of the SPR joint (Chen et al. 2003). Similarly, Huang et al. (Huang, J. Lasecki, et al. 2014) observed that at high load levels, fretting occurred between the rivet and the sheets, resulting in rivet failure. In contrast, at low loading levels, fretting occurred between the faying sheets of aluminum and steel, which lead to aluminum sheet failure. Most studies on fatigue behavior of SPR joints have indicated that, the fretting wear damage is inevitable and leads to failure of the SPR joints either by sheet failure or by rivet failure (Han, Chrysanthou, Young, et al. 2006; Han, Chrysanthou & O'Sullivan 2006; Huang, J. Lasecki, et al. 2014; Chen et al. 2003; Iyer et al. 2005). Han et al. (Han, Chrysanthou & O'Sullivan 2006) noted that the fatigue life of SPR joints in aluminum alloys was significantly improved when the faying surface interface was coated with a layer of wax-based solid surface lubricant. This wax-based lubricant reduced fretting initiated fatigue damage in the SPR joints. In addition, a study on the influence of sheet thickness on tensile strength in SPR joints of aluminum alloys showed that the thicker sheets performed better compared to thinner sheets (Han et al. 2010). This improved performance however did not translate into improved fatigue life as the SPR joints made with thicker sheets exhibited inferior fatigue life compared to SPR joints made on thinner sheets (Iyer et al. 2005). This observed reduction in fatigue performance for thicker sheets was attributed to the increase in the occurrence of fretting initiated fatigue damage.

Regarding simulation and modeling, numerous studies on SPR joints have been carried out for various materials and joint configurations. One of the pioneers on SPR joint simulation, Porcaro et al. (Porcaro et al. 2006) achieved good visual comparison between the finite element analysis (FEA) and experimental cross-sections of the joint. They achieved these results using axisymmetric model LS-DYNA with r-adaptivity, re-meshing technique, and part separation criteria based on sheet thickness. In addition, good results were obtained by employing a failure criteria based on effective strain-to-failure (Casalino et al. 2008). Recently, (Moraes et al. 2015) performed simulations by applying a temperature and strain rate sensitive material model, with a damage criterion based on void growth. Other studies with acceptable results were conducted, such as applying Gurson–Tvergaard damage model as the failure criteria (E. Atzeni et al. 2009). As the SPR process is dynamic, commonly the FEA is performed under explicit calculations, while the spring back is performed in implicit mode (Huang, J. V. Lasecki, et al. 2014; Porcaro et al. 2006; Hoang et al. 2010). However, spring back calculations of SPR using explicit analysis with mass damping have also been performed with reasonable results (Moraes et al. 2015).

Even though satisfactory results have been achieved for SPR simulations using FEA, the process simulation methods developed in literature have not been used to further understanding in regards to fretting initiated fatigue damage. Since the consensuses in literature is that fretting is the dominant factor resulting in fatigue crack initiation, the emphasis in this study is to relate the mechanics of fretting wear to SPR process. Furthermore, since fretting generally occurs at areas of high contact pressure, efforts have been made to determine contact pressure due to SPR process using finite element methods. As such, this paper presents a comprehensive study on the fatigue and fracture mechanisms and the correlation of contact pressure determined by FEA.

2. MATERIALS AND METHODS

2.1 Experimental procedures

The dissimilar aluminum lap-shear SPR test coupons were made of aluminum 61111-PFHT (post forming heat treatment) and aluminum 5754-O sheet and riveted by HENROB servo-electronic riveting equipment using 10B37 steel rivets. Each sheet measured 3.0 mm in thickness and the rivets measured 7.8 mm in diameter and 7 mm shank length. The final geometric configuration of the SPR joint test coupon is shown in Fig. 1 and the cross-section of the SPR joint is shown in Fig. 2. The load controlled fatigue tests were performed on a servo-hydraulic load frame at 40 Hz frequency in a tension-tension mode at a load ratio of R=0.1. Shims of 3.0 mm thickness were used on both ends of the lap-shear coupons to reduce the bending of the samples during testing and to balance the thickness differences.

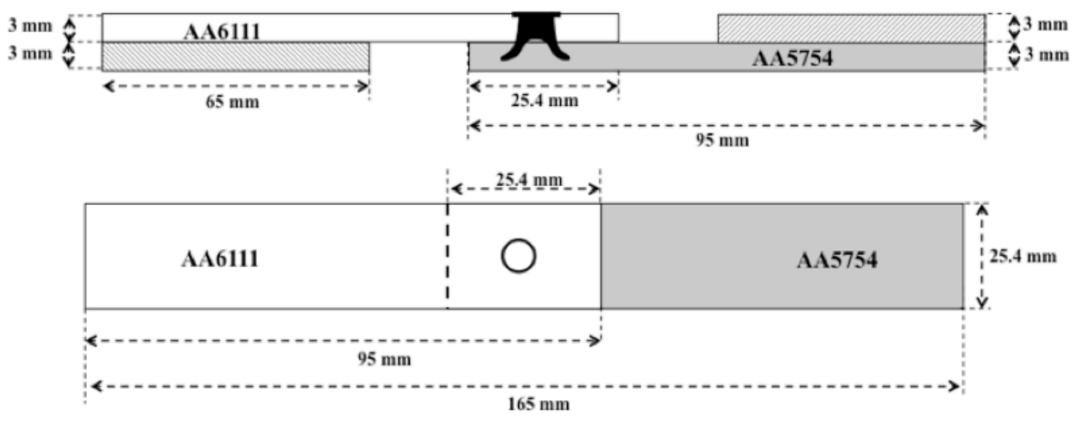

Figure 1. Self-pierce riveting test coupon.

Figure 2. Cross-section of the self-pierce riveted joint and load direction.

For metallurgical failure analysis of the SPR test coupons, the tested and untested SPR coupons were cut along the center of the coupon width parallel to loading direction. The cross-sectioned samples were then cold mounted in an epoxy, ground and a final polishing was done using a 0.5 μm colloidal silica. The macrographs of the samples were performed using a Keyence VHX100 digital optical microscopy.

2.2 Finite element methods

Numerical simulations were performed using the commercial solver Abaqus. Since the SPR is a dynamic process, the explicit solver was chosen. SPR joints can be approximated as axisymmetric and many studies have been done using 2D elements (Casalino et al. 2008; Porcaro et al. 2006; E Atzeni et al. 2009). Nevertheless, 3D elements with reduced integration were used in order to take advantage of a better contact formulation included in Abaqus (named General Contact). Elements of the rivet are 0.2 x 0.2 mm on average, and elements of the sheets are 0.05 x 0.05 mm on X-Y plane. Depth of the element depends on how far the element is from the Y-axis, as the mesh was built by sweeping 7.5 degrees around the Y-axis. As a result, the model appears to have a "wedge" geometry. The initial mesh configuration can be seen in Fig. 3.

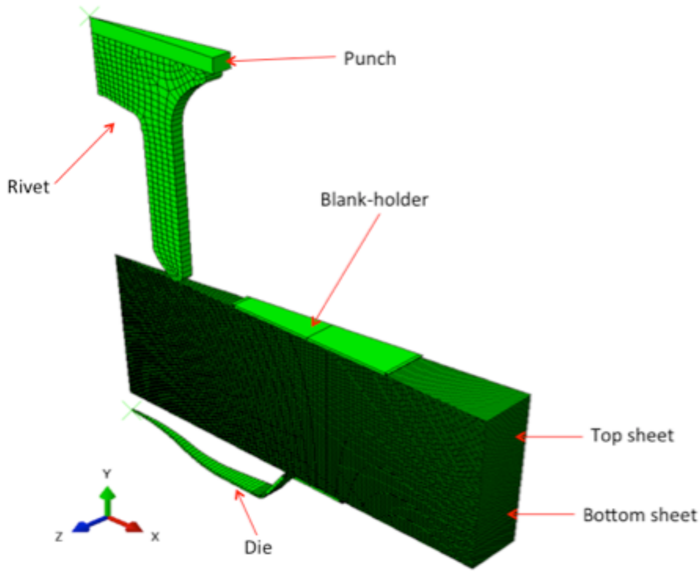

Figure 3. Initial configuration of the SPR "wedge" model

An isotropic material hardening model was applied for both the sheets and the rivet. Stress-strain curves for various materials were obtained from literature: aluminum alloy 6011 (top sheet) (Kim et al. 2010); aluminum alloy 5754 (bottom sheet) (Ozturk et al. 2011); and HB37 (rivet) (Hall et al. 2014). Die and punch were modeled as rigid bodies while the back-holder was modeled as purely elastic with very high elastic modulus, which allows it to be nearly as stiff as a rigid body, however, this allows pressure loads to be easily applied on its top surface. In order to allow the rivet to pierce through the top sheet, elements were deleted according to the Johnson-Cook damage criterion. Damage evolution was selected to rapidly decrease the energy of the element to be killed before it is deleted, avoiding numerical complications due to energy equilibrium. Equations (1) and (2) are the governing equations of Johnson-Cook damage criterion implemented in Abaqus. Complete damage occurs when the damage parameter, ω, reaches unity:

$$\omega = \sum\left(\frac{\Delta\bar{\varepsilon}^{pl}}{\bar{\varepsilon}_f^{pl}}\right) \tag{1}$$

where $\Delta\bar{\varepsilon}^{pl}$ is an increment of plastic strain, $\bar{\varepsilon}_f^{pl}$ is the strain at damage initiation, and the summation is performed at each increment of the analysis. $\bar{\varepsilon}_f^{pl}$ is defined in Equation (2):

$$\bar{\varepsilon}_f^{pl} = \left[d_1 + d_2 \exp\left(d_3 \frac{p}{q}\right)\right]\left[1 + d_4 \ln\left(\frac{\dot{\bar{\varepsilon}}^{pl}}{\dot{\varepsilon_0}}\right)\right](1 + d_5\hat{\theta}) \tag{2}$$

Constants $d_{1\text{-}5}$ are failure parameters, $\dot{\varepsilon_0}$ is the reference strain rate, $\hat{\theta}$is the non-dimensional temperature, p is the pressure stress and q is the Mises stress. Since parameters d_4 and d_5 are related to strain rate sensitivity and temperature, respectively, they were set to zero during the model calibration because the material model chosen is neither strain rate nor temperature dependent. Failure parameters and friction were calibrated through visual comparison between simulation and cross-section of the SPR joint.

Following the calibration stage, a spring-back study was performed. This simulation was performed using the explicit code in order to keep contact histories intact. This type of spring-back was achieved releasing the punch and blank-holder slowly, applying a viscous pressure load to damp dynamic oscillations and to achieve quasi-static equilibrium.

3. RESULTS AND DISCUSSION

3.1 Fatigue tests and failure mode analysis

Figure 4 is the plot of fatigue test results of the dissimilar aluminum SPR joints. Two prominent modes of failure were observed: failure of the rivets and failure of the top sheet. The failure of the rivets occurred in coupons tested above 2000 N load amplitude. In SPR coupons tested at load amplitudes below 2000 N, failure occurred through the top AA6111 sheet. In addition, at a load amplitude of 450 N, majority of the SPR coupons had a run-out. It is noted that, this paper focuses on the fatigue and fracture of the SPR joints in the high cycle fatigue regime (Nf > 10^6 cycles, highlighted in Fig.4), hence the failure mode of SPR joints with fatigue life below 10^6 cycles will not be discussed.

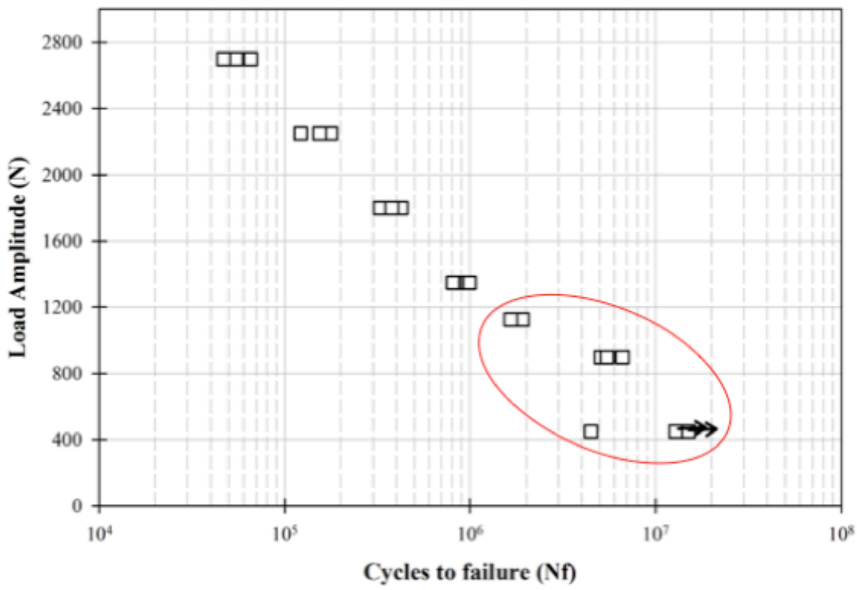

Figure 4. Fatigue plot of dissimilar aluminum self-pierce riveted joint

Figure 5 represents the failure modes of the SPR coupons tested at 900 N and 1125 N load amplitudes, respectifully. Fretting wear was observed on the faying surface (bottom surface of the top sheets) of the top and bottom sheets of the fracture samples. In Fig. 5(a) and (b) the bold arrows represent the dominant fretting regions on the top sheet faying surfaces. In both the failure modes, the fatigue cracks propagated away from the rivet as seen in Fig. 5(c) and Fig. 5(d).

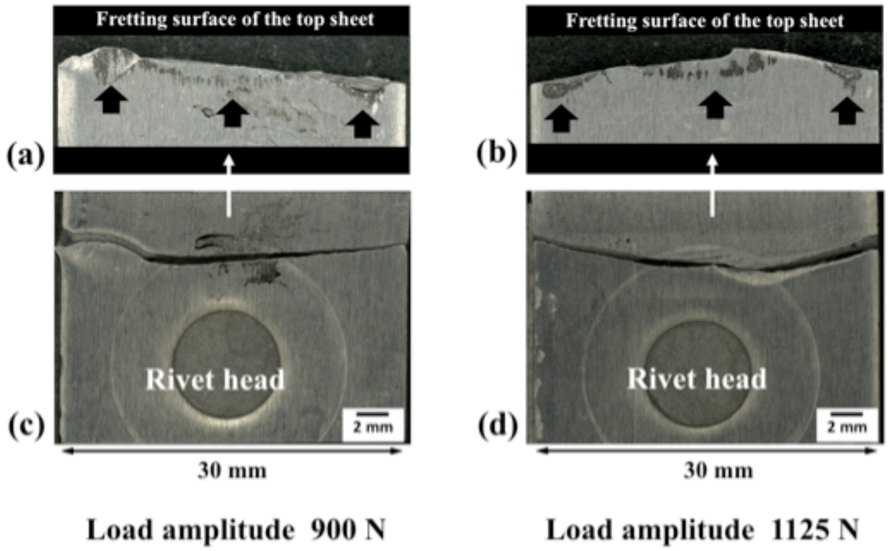

Figure 5. Failure mode of the SPR joint subjected to fatigue loading.

Figure 6 shows the cross-section of the failed SPR coupons. Figure 6(a) and Fig. 6(c) are the macrographs showing the top sheet failure in SPR joints tested at 900 N and 1125 N load amplitude respectively. Figure 6(b) and Fig. 6(d) are the cross-sections of the above SPR coupons along BB mounted in epoxy. Shear lips were optically observed in both the failure modes. In SPR coupons tested at 900 N load amplitude, the shear lip was observed on the corner of the specimen and in SPR coupons tested at 1125 N load amplitude, the shear lip was observed close to center of the sheet width as seen in Fig. 6(a) and (b) respectively. The cross sections of the two specimens shown are illustrated in Fig. 6(b) and (d).

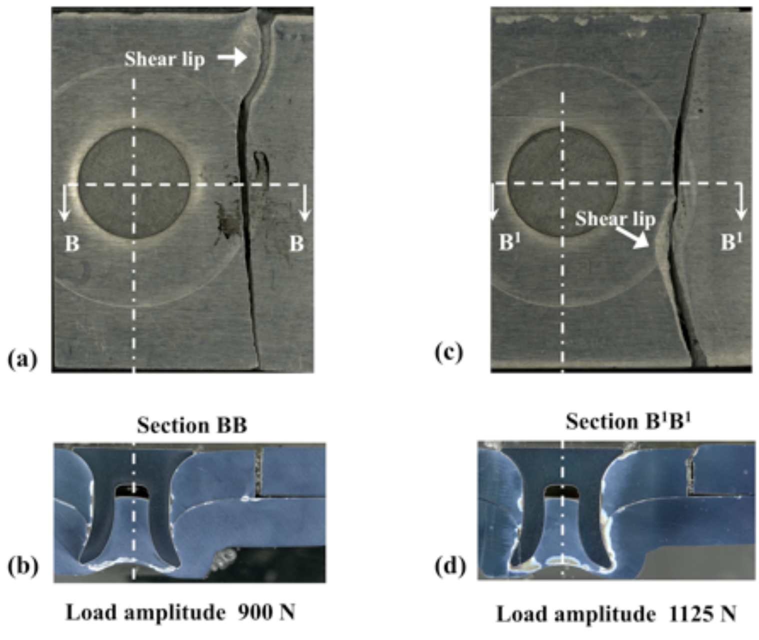

Figure 6. Comparison of the location of the fatigue crack initiation in relation to the rivet.

3.2 Finite element analysis

As noted previously, parameters d_2 and d_3 are related to the stress triaxiality and are key to obtaining a good visual comparison. Parameters d_1, d_2 and d_3 were found to be 0.18, 2, and 0.2 respectively. Moreover, coefficients of friction are also important and can change simulations results considerably. In addition, the coefficients of friction found suitable for this work are shown in Table 1.

Table 1.Coefficients of friction used in the FEA.

Contact pair	Coefficient of friction
Punch/Rivet	0.4
Rivet/ Top sheet	0.12
Rivet/ Bottom sheet	0.12
Blank-holder/ Top sheet	0.2
Top sheet/ Bottom sheet	0.2
Top sheet/ Top sheet	0.15
Die/ Bottom sheet	0.15

Figure 7 shows the final configuration of the simulation after spring-back compared to the experimental cross-section. On the left, the edges of the rivet, top and bottom sheets of the simulation are shown, while the die, punch and blank-holder were omitted for a clearer image. On the right side, the actual cross section of the riveted joint is shown. As one can observe, good agreement between the simulation and experimental joint was achieved.

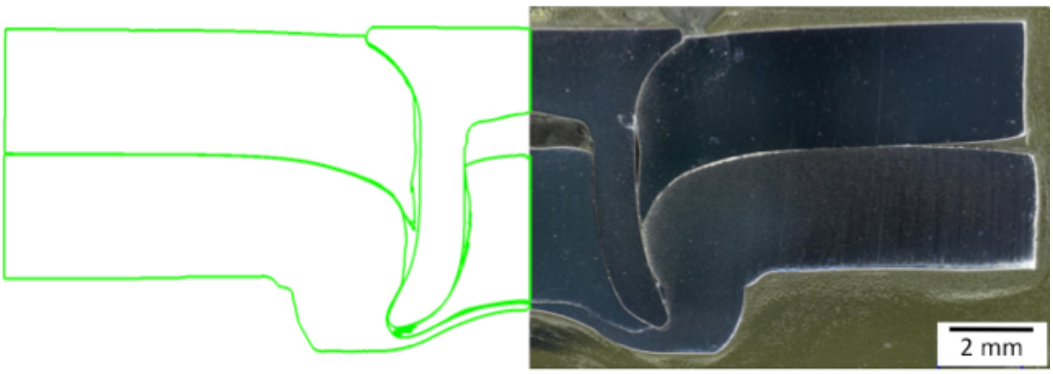

Figure 7. Visual validation of the model (on the left) against the experimental cross section (on the right).

Figure 8 shows the evolution of residual stress that occur during the SPR process. Figure 8a shows the FEA results just after the SPR process and Fig. 8b shows the results just after the release of the punch and blank-holder. Figure 8c shows the FEA results after the release of the die. It can be readily observed how residual stresses decrease after spring-back. In addition, there is more residual stresses near the rivet location, as this may indicate the reason of failure of the coupons tested at higher load, where failure occurs at the rivet.

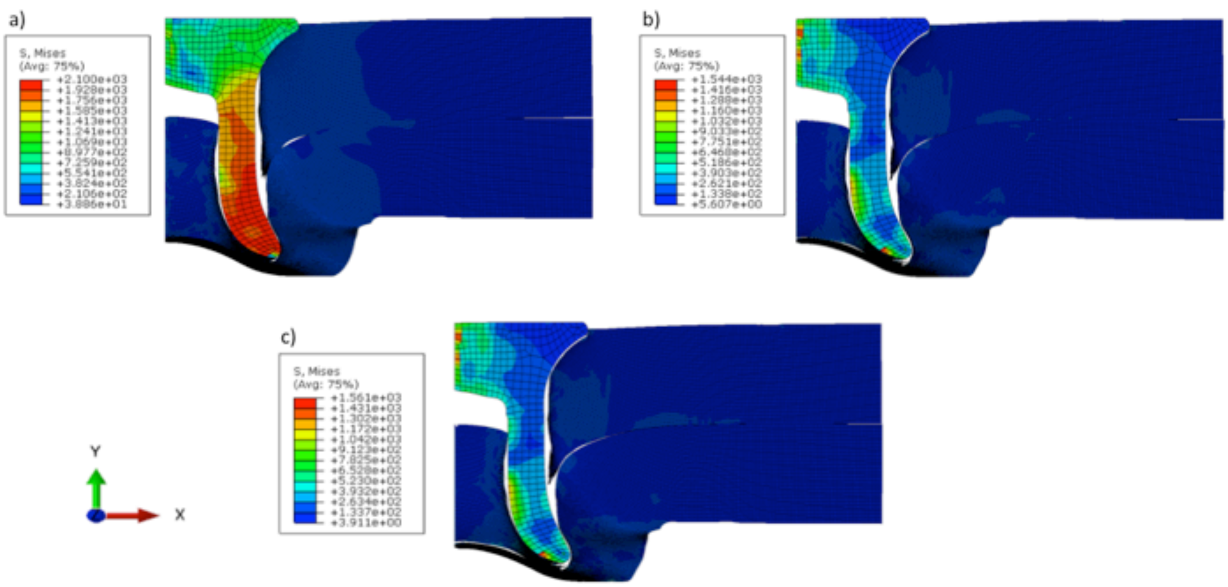

Figure 8. Evolution of residual stress: a) just after the SPR process, b) after the release of the punch and blank-holder and c) after the release of the die.

Once the final geometry was validated against the experimental cross-section, contact pressure was evaluated and compared to the experimental location fretting initiated fatigue. Figure 9a shows the cross-section of the failed specimen tested at 900N, and Fig. 9 b shows the contact pressure of the simulation after the spring-back. The arrow indicates where the highest contact pressure between top and bottom sheets is located as determined by the FEA. Moreover, the location of the highest contact pressure is located away from the rivet and correlates well with the fretting location determined experimentally.

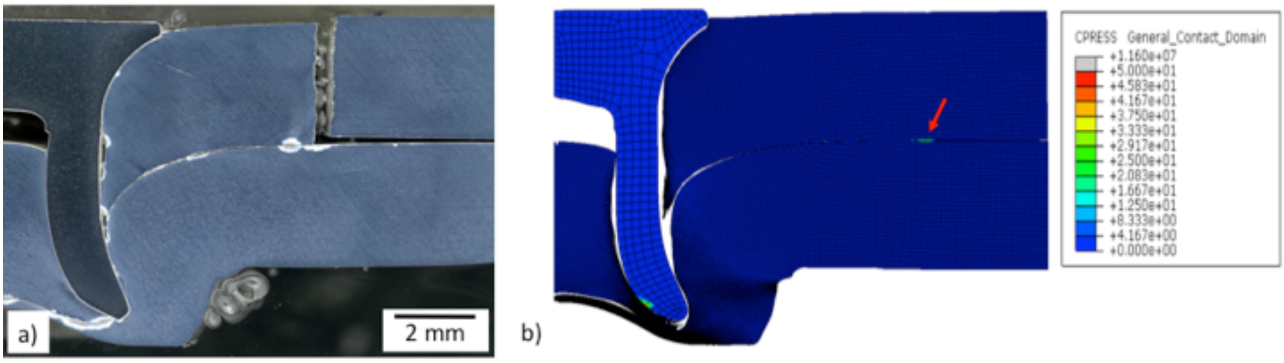

Figure 9. Correlation between: a) failure location of experimental cross-section, and (b) contact pressure from simulation results.

4. CONCLUSIONS

Efforts in correlating residual stresses, contact forces and fatigue damage of dissimilar aluminum alloy sheets joined via SPR was conducted. High cycle fatigue results suggest that fretting wear initiated fatigue cracks that lead to failure of the joint away from the rivet. FEA of the SPR process showed the highest contact pressure was located near the location of fatigue crack initiation. As such, in this present study, we have shown that the deformation that occurs due to the SPR process creates high contact stresses that in the case of 3mm thick sheets of aluminum alloy, leads to detrimental fatigue crack initiation and propagation away from the existing stress concentration created by the rivet.

5. ACKNOWLEDGEMENTS

This work utilized resources owned and maintained by the Central Analytical Facility, which is supported by The University of Alabama.

6. REFERENCES

Abe, Y., Kato, T. & Mori, K., 2009. Self-piercing riveting of high tensile strength steel and aluminium alloy sheets using conventional rivet and die. *Journal of Materials Processing Technology*, 209, pp.3914–3922.

Atzeni, E., Ippolito, R. & Settineri, L., 2009. CIRP Annals - Manufacturing Technology Experimental and numerical appraisal of self-piercing riveting. , 58, pp.17–20.

Atzeni, E., Ippolito, R. & Settineri, L., 2009. Experimental and numerical appraisal of self-piercing riveting. *CIRP Annals - Manufacturing Technology*, 58(1), pp.17–20.

Barnes, T.A. & Pashby, I.R., 2000a. Joining techniques for aluminium spaceframes used in automobiles Part I - solid and liquid phase welding. , 99, pp.62–71. Available at: http://wrap.warwick.ac.uk/13593/.

Barnes, T.A. & Pashby, I.R., 2000b. Joining techniques for aluminium spaceframes used in automobiles Part II Đ adhesive bonding and mechanical fasteners. , 99, pp.72–79.

Cai, W., Wang, P.C. & Yang, W., 2005. Assembly dimensional prediction for self-piercing riveted aluminum panels. , 45, pp.695–704.

Casalino, G., Rotondo, a. & Ludovico, a., 2008. On the numerical modelling of the multiphysics self piercing riveting process based on the finite element technique. *Advances in Engineering Software*, 39(9), pp.787–795.

Chen, Y.K. et al., 2003. Fretting wear in self-piercing riveted aluminium alloy sheet. , 255, pp.1463–1470.

Fu, M. & Mallick, P.K., 2003. Fatigue of self-piercing riveted joints in aluminum alloy 6111. , 25, pp.183–189.

Hall, S.N. Van, Findley, K.O. & Campbell, A.M., 2014. Evaluating the performance of current self-pierce rivet technology for the joining of high strength steel and aluminum alloys. In *ASME 2014 International Manufacturing Science and Engineering Conference*. pp. 1–5.

Han, L., Chrysanthou, a., Young, K.W., et al., 2006. Characterization of fretting fatigue in self-piercing riveted aluminium alloy sheets. *Fatigue and Fracture of Engineering Materials and Structures*, 29(8), pp.646–654.

Han, L. & Chrysanthou, a., 2008. Evaluation of quality and behaviour of self-piercing riveted aluminium to high strength low alloy sheets with different surface coatings. *Materials and Design*, 29(2), pp.458–468.

Han, L., Chrysanthou, a. & O'Sullivan, J.M., 2006. Fretting behaviour of self-piercing riveted aluminium alloy joints under different interfacial conditions. *Materials and Design*, 27(3), pp.200–208.

Han, L., Chrysanthou, a. & Young, K.W., 2007. Mechanical behaviour of self-piercing riveted multi-layer joints under different specimen configurations. *Materials and Design*, 28(7), pp.2024–2033.

Han, L., Thornton, M. & Shergold, M., 2010. A comparison of the mechanical behaviour of self-piercing riveted and resistance spot welded aluminium sheets for the automotive industry. *Materials and Design*, 31(3), pp.1457–1467. Available at: http://dx.doi.org/10.1016/j.matdes.2009.08.031.

Hoang, N.H. et al., 2010. Self-piercing riveting connections using aluminium rivets. *International Journal of Solids and Structures*, 47(3-4), pp.427–439.

Huang, L., Lasecki, J., et al., 2014. Fatigue and Fretting of Mixed Metal Self-Piercing Riveted Joints. In *ASME International Mechanical Engineering Congress 2014*. pp. 1–6.

Huang, L., Lasecki, J. V., et al., 2014. Finite Element Modeling of Dissimilar Metal Self-piercing Riveting Process. *SAE International Journal of Materials and Manufacturing*, 7(3), pp.5–12. Available at: http://www.scopus.com/inward/record.url?eid=2-s2.0-84898076765&partnerID=tZOtx3y1.

Hurricks, P.L., 1970. The mechanism of fretting — A review. *Wear*, 15(6), pp.389–409.

Iyer, K. et al., 2005. Fatigue of single- And double-rivet self-piercing riveted lap joints. *Fatigue and Fracture of Engineering Materials and Structures*, 28(11), pp.997–1007.

Kim, D. et al., 2010. Formability evaluation of friction stir welded 6111-T4 sheet with respect to joining material direction. *International Journal of Mechanical Sciences*, 52(4), pp.612–625. Available at: http://dx.doi.org/10.1016/j.ijmecsci.2010.01.001.

Litherland, H., 1998. Joints in Aluminum: INALCO' 98 Proceedings. In *Joints in Aluminum: INALCO' 98 Proceedings*. Cambridge: Woodhead Publishing, pp. 135–147.

Miller, W.S. et al., 2000. Recent development in aluminium alloys for the automotive industry. , 280, pp.37–49.

Moraes, J.F.C., Jordon, J.B. & Bammann, D.J., 2015. Finite Element Analysis of Self-Pierce Riveting in Magnesium Alloys Sheets. , 137(April).

Mortimer, J., 2001. Jaguar uses X350 car to pioneer use of self-piercing rivets. *Industrial Robot: An International Journal*, 28, pp.192–198.

Ozturk, F., Pekel, H. & Halkaci, H.S., 2011. The effect of strain-rate sensitivity on formability of AA 5754-O at cold and warm temperatures. *Journal of Materials Engineering and Performance*, 20(1), pp.77–81.

Pickin, C.G., Young, K. & Tuersley, I., 2007. Materials & Design Joining of lightweight sandwich sheets to aluminium using self-pierce riveting. , 28, pp.2361–2365.

Porcaro, R. et al., 2006. Self-piercing riveting process : An experimental and numerical investigation. , 171, pp.10–20.

Sun, X., Stephens, E. V & Khaleel, M.A., 2007. International Journalof Fatigue Fatigue behaviors of self-piercing rivets joining similar and dissimilar sheet metals. , 29, pp.370–386.

Waterhouse, R.B., 1984. Fretting wear. *Wear*, 100(1–3), pp.107–118. Available at: http://www.sciencedirect.com/science/article/pii/0043164884900085.

7. RESPONSIBILITY NOTICE

The authors are the only responsibles for the printed material included in this paper.